

Destabilization by noise of transverse perturbations to heteroclinic cycles: a simple model and an example from dynamo theory

BY J. R. GOG¹, I. OPREA²†, M. R. E. PROCTOR¹
AND A. M. RUCKLIDGE¹

¹*Department of Applied Mathematics and Theoretical Physics,
University of Cambridge, Cambridge CB3 9EW, UK*

²*Faculty of Mathematics, University of Bucharest, Str. Academiei 14,
Sector 1, Bucharest, Romania*

Received 15 October 1998; revised 9 March 1999; accepted 5 May 1999

We show that transverse perturbations from structurally stable heteroclinic cycles can be destabilized by surprisingly small amounts of noise, even when each individual fixed point of the cycle is stable to transverse modes. A condition that favours this process is that the linearization of the dynamics in the transverse direction be characterized by a non-normal matrix. The phenomenon is illustrated by a simple two-dimensional switching model and by a simulation of a convectively driven dynamo.

Keywords: transverse instability; noise-induced instability;
non-normal dynamics; heteroclinic cycle; dynamo theory

1. Introduction

There has been a great deal of recent interest in the instabilities of low-dimensional, but temporally complex, orbits embedded in invariant subspaces of a higher-dimensional phase space. Such orbits can become unstable to perturbations within this subspace or orthogonal to it; the latter instability, known as a *transverse* instability, typically involves different parts of the subspace having different local stability properties with regard to the transverse modes, with the growth rate of transverse perturbations changing from negative to positive as a result of varying a parameter (Ashwin *et al.* 1996; Chossat *et al.* 1997). Although a natural definition of instability might be the existence of a mean positive growth rate when averaged over long times, we show in this paper that orbits which are stable by this definition may be destabilized by the addition of a small but finite amount of random noise to the dynamics within the invariant subspace. We shall consider the particular situation in which the underlying orbit is a structurally stable heteroclinic cycle, connecting a number of

† Present address: Department of Mathematics, Colorado State University, Fort Collins, CO 80523, USA.

equilibrium points P_1, P_2, \dots, P_n in the phase space, and make the surprising observation that this noise-induced instability can occur even if each equilibrium point in the cycle is linearly stable to transverse perturbations.

If the transverse perturbation vanishes, the orbit at large times spends a long time ΔT_j (the *transit time*) in the vicinity of each P_j ; if the ΔT_j are long enough for transient effects of the (rapid) movement between the equilibrium points to be ignored, then the exponential growth of the transverse mode when the orbit is near P_j is well approximated by $e^{\text{Re } \lambda^{(j)} \Delta T_j}$, where $\lambda^{(j)}$ is the eigenvalue with largest real part of the transverse stability problem for the equilibrium point P_j . Then the mean growth rate γ is easily seen to be well approximated by

$$\gamma = \frac{\sum_j \text{Re } \lambda^{(j)} \Delta T_j}{\sum_j \Delta T_j}. \quad (1.1)$$

It is clear from this expression that provided that all the ΔT_j are sufficiently large for it to be valid, then it is sufficient for stability (instability) that all the $\lambda^{(j)}$ have negative (positive) real part. (When the real parts of the $\lambda^{(j)}$ are not all of one sign then stability cannot be determined without knowledge of the dynamics near the equilibrium points.)

We now suppose that the transit times are still long compared with the times taken to move from the neighbourhood of one equilibrium point to the next, but not so long that transients in the transverse dynamics can be neglected. We must distinguish between normal and non-normal transverse dynamics. A matrix A is *normal* if it possesses a complete set of orthogonal eigenvectors, or, equivalently, if $AA^\dagger = A^\dagger A$ (where A^\dagger is the complex conjugate transpose of A). If A is normal, then the linear system $\dot{z} = Az$ has solutions that evolve as

$$|z(t)|^2 = \sum_i c_i^2 e^{2 \text{Re } \lambda_i t},$$

where the λ_i are eigenvalues of A , and the c_i^2 are constants. Then if the eigenvalues all have negative real part, the amplitude of the disturbance decreases exponentially even during periods of transient behaviour, and so the criterion for stability given above remains valid (in fact, as can easily be seen, the system is more stable for shorter transit times). However, the situation is quite different when the transverse dynamics is *non-normal*; in this case, even when all the eigenvalues have negative real part, there can be transient growth in the amplitude of the disturbance (see, for example, Trefethen 1997; Farrell & Ioannou 1994). If then the transit times ΔT_j are sufficiently short, we can find that growth can occur as a result of the switching, as transient growth can occur near each P_j .

If the underlying cycle is heteroclinic, then in a real physical system the presence of external disturbance (conveniently modelled as additive noise) will prevent the transit times becoming indefinitely long as the cycle is approached. Stone & Holmes (1990), Lythe & Proctor (1993) and others have shown that in the presence of noise the cycle becomes noisily periodic, with a well-defined mean period that scales logarithmically with the noise level. This natural perturbation, then, is a way of controlling the transit times, and thus of destabilizing the system to transverse modes by the process described above. The aim of this paper is to quantify and illustrate the above mechanism in two ways. We firstly (§ 2) analyse a very simple system

with just two equilibrium points, with two-dimensional transverse dynamics, which allows us to calculate the growth rates in closed form; this is then elaborated by adding stochastic fluctuations. In §3 we investigate a (truncated) system of partial differential equations (PDEs) that exhibit the destabilization phenomenon: thermal convection in a layer of electrically conducting fluid. The transverse instability in this case is the so-called dynamo instability, which leads to growing magnetic perturbations. The invariant subspace containing the structurally stable heteroclinic cycle is characterized by having zero magnetic field. This system is investigated numerically, and the results show good qualitative agreement with the general formulae suggested by the simpler system. We conclude in §4 with a discussion of the nonlinear behaviour of the instabilities.

This and all subsequent analysis ignores any growth that might occur when switching between the equilibrium points of the cycle. Such growth would be independent of the transit times near the equilibrium points, and could lead to instability even when the transverse dynamics near the equilibrium points is normal, provided the transit times are short enough.

2. A simple model system

(a) Analysis for fixed switching times

Before embarking on the detailed model of §3, we illustrate the main ideas that lie behind this model by considering a very simple second-order non-autonomous ordinary differential equation (ODE). We are trying to represent the idea of a finite number of *different* transverse instability problems (one for each equilibrium point on the cycle) with rapid switching between the points. The simplest case would seem to be two such problems and, because of the requirement of non-normality, we require each problem to have second-order dynamics. We are thus led to consider a system of the form, with $\mathbf{z} \in \mathbb{R}^2$:

$$\dot{\mathbf{z}} = A(t)\mathbf{z}, \quad (2.1)$$

where A is a 2×2 real matrix. If we define a sequence of *switching times* T_n : $n = 0, 1, 2, \dots$, with $T_0 = 0$ (so $\Delta T_n = T_n - T_{n-1}$), then $A(t)$ has the form

$$A = \begin{cases} A_1 \equiv \begin{pmatrix} -\lambda & a^2 \\ -1 & -\lambda \end{pmatrix}, & \text{when } T_{2n} < t < T_{2n+1}, \\ A_2 \equiv \begin{pmatrix} -\lambda & 1 \\ -a^2 & -\lambda \end{pmatrix}, & \text{when } T_{2n+1} < t < T_{2n+2}, \end{cases} \quad (2.2)$$

where $\lambda > 0$ and λ and a^2 are constant. We think of λ as small, so that between the T_n the trajectory of \mathbf{z} is close to an ellipse with ratio of major to minor axis equal to a , but decays slowly towards the origin. The two forms of A give the same sense of rotation, but with the two sets of major axes at 90° as in figure 1a.

We regard the existence of finite transit times ΔT_n as being due to noise in the underlying dynamical system. In the absence of noise, the transit times would tend geometrically to infinity if the underlying heteroclinic cycle is asymptotically stable (Krupa & Melbourne 1995). In due course we shall regard ΔT_n as a random variable

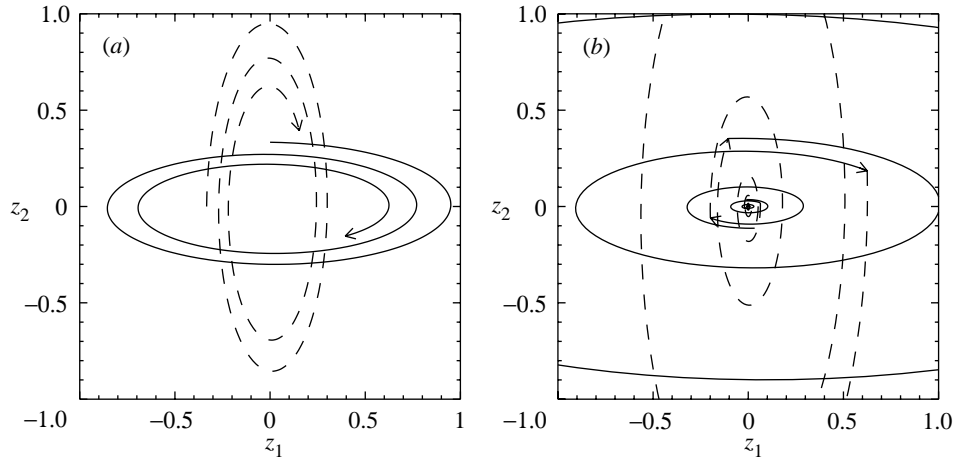


Figure 1. (a) $\dot{\mathbf{z}} = A_1\mathbf{z}$ (solid line) and $\dot{\mathbf{z}} = A_2\mathbf{z}$ (dashed line), with $a = 3$ and $\lambda = 0.1$: trajectories spiral (in a clockwise sense) into the origin. (b) Switching between $\dot{\mathbf{z}} = A_1\mathbf{z}$ (solid line) and $\dot{\mathbf{z}} = A_2\mathbf{z}$ (dashed line) with a switching time of 1.15 times the basic period: trajectories grow on average.

with an appropriate probability distribution, but to begin with we assume that the switching intervals are all the same, so that $T_n = nT$, say (see figure 1b).

We suppose that at $t = 0$, $\mathbf{z} = \mathbf{z}_0$. Then it is easy to show that

$$\mathbf{z}(T) = M_1\mathbf{z}_0, \quad \mathbf{z}(2T) = M_2M_1\mathbf{z}_0, \quad (2.3)$$

where

$$M_1 = e^{-\lambda T} \begin{pmatrix} \cos aT & a \sin aT \\ -(1/a) \sin aT & \cos aT \end{pmatrix}, \quad M_2 = e^{-\lambda T} \begin{pmatrix} \cos aT & (1/a) \sin aT \\ -a \sin aT & \cos aT \end{pmatrix}. \quad (2.4)$$

Thus after one complete cycle $2T$, the map taking $\mathbf{z}(0)$ to $\mathbf{z}(2T)$ is M_2M_1 :

$$M_2M_1 = e^{-2\lambda T} \begin{pmatrix} \cos^2 aT - (1/a^2) \sin^2 aT & (a + (1/a)) \sin aT \cos aT \\ -(a + (1/a)) \sin aT \cos aT & \cos^2 aT - a^2 \sin^2 aT \end{pmatrix}. \quad (2.5)$$

The stability of the system to transverse perturbations now depends on the eigenvalues of (2.5). The characteristic equation is

$$\rho^2 - e^{-2\lambda T}[2 - 4\eta^2]\rho + e^{-4\lambda T} = 0, \quad (2.6)$$

where $\eta = \frac{1}{2}(a + (1/a)) \sin aT$. The solutions are

$$\rho_{\pm} = -e^{-2\lambda T}[|\eta| \pm \sqrt{\eta^2 - 1}]^2, \quad (2.7)$$

so the eigenvalues ρ_{\pm} depend only on λT and η . The quantity η may be greater or less than unity, and so the eigenvalues may be real or complex.

If $|\eta| < 1$, then

$$\rho_{\pm} = -e^{-2\lambda T}[|\eta| \pm i\sqrt{1 - \eta^2}]^2, \quad (2.8)$$

and so $|\rho_{\pm}| = e^{-2\lambda T} < 1$ if $\lambda T > 0$. Hence we have decay in this case, and the system is stable to transverse perturbations. On the other hand, if $|\eta| \geq 1$, we have real eigenvalues, whose product is $e^{-4\lambda T}$. Thus the eigenvalue of smaller modulus (ρ_-) satisfies $|\rho_-| < e^{-2\lambda T} < 1$, while the other eigenvalue ρ_+ is

$$\rho_+ = -e^{-2\lambda T} [|\eta| + \sqrt{\eta^2 - 1}]^2. \quad (2.9)$$

We therefore have instability if $|\rho_+| > 1$, or if

$$\lambda T < \cosh^{-1} \eta. \quad (2.10)$$

Thus the stability boundary in (T, η) -space is given by $\lambda T = \cosh^{-1} \eta$. Note that since $|\eta| \leq \frac{1}{2}(a + (1/a))$, there can be no instability if $\lambda T > |\ln a|$.

It is instructive for what comes later in the paper to re-express the instability criterion (2.10) by giving an expression for the growth rate γ . For fixed a we have the relation

$$\gamma = \begin{cases} \frac{1}{T} \cosh^{-1} \eta - \lambda, & \text{for } |\eta| > 1, \\ -\lambda, & \text{for } |\eta| < 1, \end{cases} \quad (2.11)$$

which takes the form shown in figure 2*a, b* for two different values of a and $\lambda = 0.1$ (growth rates for other values of λ can be found by shifting those shown). We see that if we fix λ , there are a finite number of disjoint intervals of T giving instability (though instability is impossible for any T if λ is sufficiently large). These intervals are neighbourhoods of times for which the system makes an odd number of quarter turns at each equilibrium point, so that the system can take best advantage of the transient growth offered by the elliptical shape of the decaying orbits (as in figure 1*b*).

We can, of course, extend these results to the case where the eigenvalues of A_1 and A_2 are real. A particular though marginal example is provided by taking the limit $a \rightarrow 0$, when A_1, A_2 represent simple shears with damping and

$$M_1 = e^{-\lambda T} \begin{pmatrix} 1 & 0 \\ -T & 1 \end{pmatrix}, \quad M_2 = e^{-\lambda T} \begin{pmatrix} 1 & T \\ 0 & 1 \end{pmatrix}. \quad (2.12)$$

We also have $\eta = \frac{1}{2}T$. Thus the relation (2.11) is replaced by

$$\gamma = \begin{cases} \frac{1}{T} \cosh^{-1} \frac{1}{2}T - \lambda, & \text{for } T > 2, \\ -\lambda, & \text{for } T < 2, \end{cases} \quad (2.13)$$

as plotted in figure 2*c*. Because the eigenvalues are real there is now only one extremum to the stability boundary.

The foregoing analysis assumes that our putative heteroclinic cycle has only two equilibrium points. However, it can happen that in a dynamical system with symmetry the relevant equilibrium points possess images under a symmetry operation, forming a heteroclinic network. A noisy orbit close to the heteroclinic cycle may then visit any of the images of the equilibrium point. To model this random process, whose details are intimately bound up with the effects of the noise on the passage time, we now extend our model system so that

$$A = \begin{cases} A_1 \text{ or } \tilde{A}_1 \equiv A_2^\dagger, & \text{for } T_{2n} < t < T_{2n+1}, \\ A_2 \text{ or } \tilde{A}_2 \equiv A_1^\dagger, & \text{for } T_{2n+1} < t < T_{2n+2}, \end{cases} \quad (2.14)$$

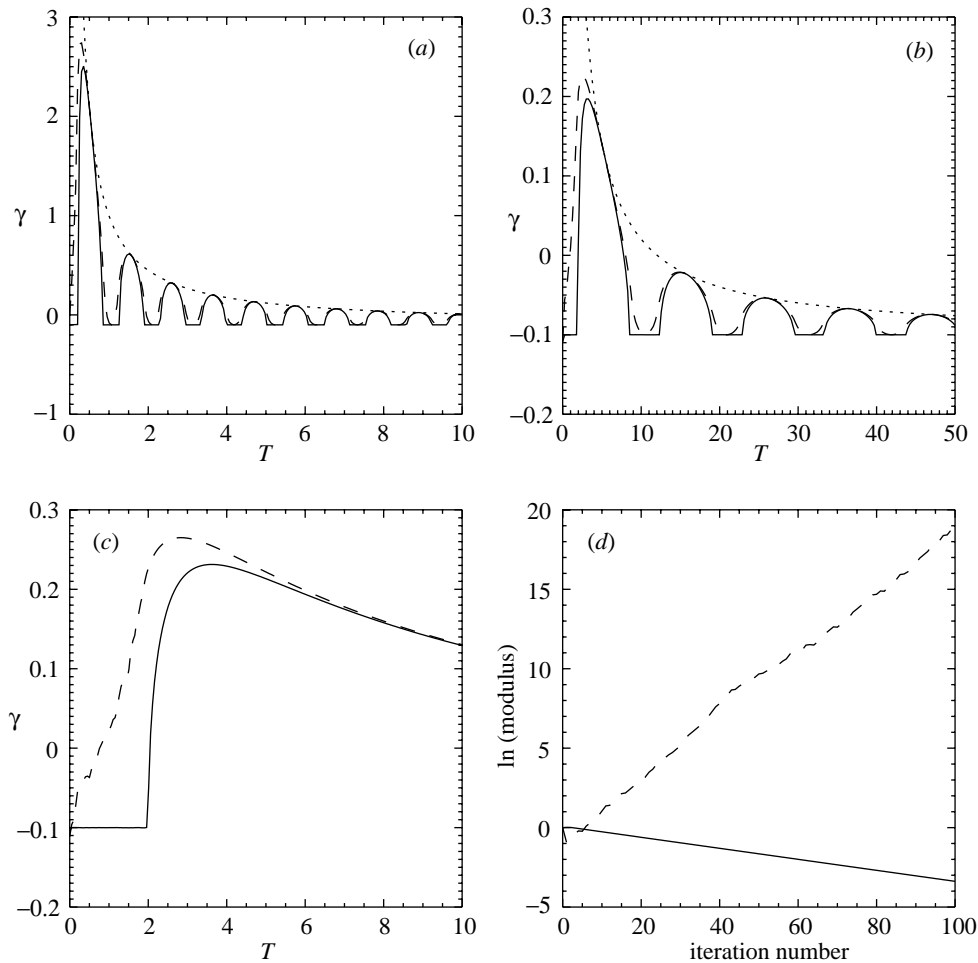


Figure 2. Results for the switching model with constant switching time T . The first three graphs show growth rate γ as a function of T for $\lambda = 0.1$ and (a) $a = 3.0$, (b) $a = 0.3$, (c) $a = 0$. In each graph the full line shows the deterministic case and the dashed line the random case. The dotted lines in (a) and (b) show the upper bound $|\ln a|/T - \lambda$. (d) shows the growth of an initial unit vector in the deterministic case (full line) and random case (dashed line), for $a = 0.3$, $T = 7.8$.

with equal probability in each case, independent of previous choices. Integrating for a period T leads by analogy to the new multiplier matrices as equally likely alternatives to M_1 , M_2 in (2.3):

$$\tilde{M}_1 = e^{-\lambda T} \begin{pmatrix} \cos aT & -a \sin aT \\ (1/a) \sin aT & \cos aT \end{pmatrix}, \quad \tilde{M}_2 = e^{-\lambda T} \begin{pmatrix} \cos aT & -(1/a) \sin aT \\ a \sin aT & \cos aT \end{pmatrix}. \quad (2.15)$$

Note that for $\lambda = 0$, \tilde{M}_1, \tilde{M}_2 are the inverses of M_1, M_2 . Then assuming the cycle times are all equal to T , we have with equal probability one of the following four multipliers: $M_2 M_1$, $\tilde{M}_2 \tilde{M}_1$, $M_2 \tilde{M}_1$, $\tilde{M}_2 M_1$. The first and fourth of these are transpositions of each other, while the second and third are symmetric and have the same

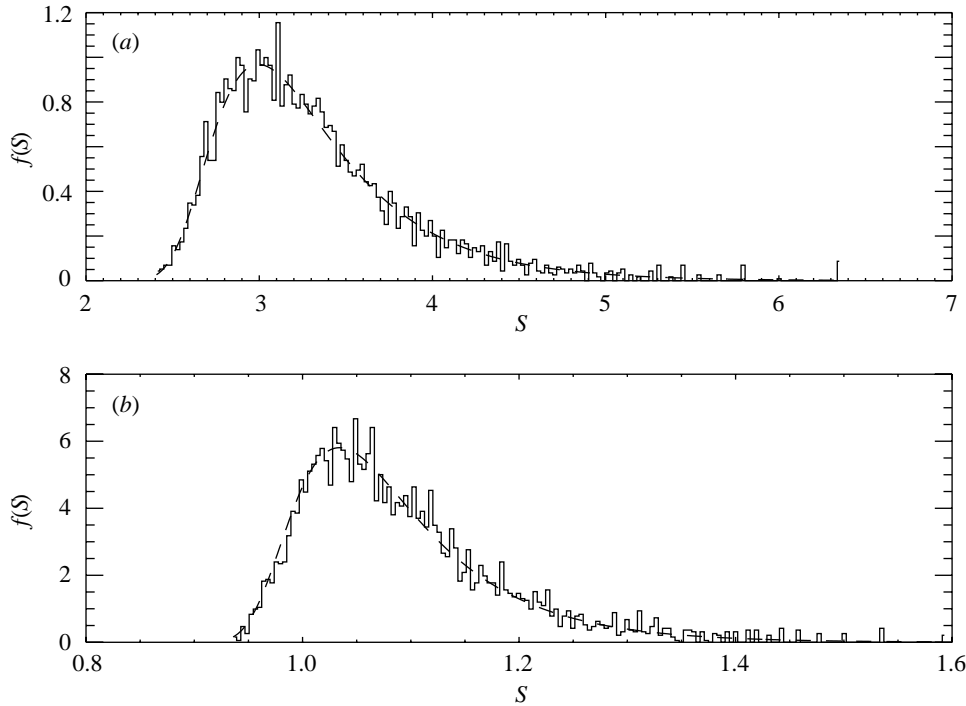


Figure 3. The density function of the probability distribution given by (2.18): (a) $\delta = 2.0$, $\lambda_u = 2.0$; (b) $\delta = 500.0$, $\lambda_u = 12.0$, with noise $\varepsilon = 10^{-2}$ in both cases. The histograms show the distribution of 5000 sample points.

eigenvalues, although their eigenvectors are different. In figure 2*a–c*, we show the (numerically computed) growth rates as functions of T for the same values of a and λ as in the non-random case described above. In this simple model the maxima of the growth rate curve are not affected by the fluctuations. For other values the random switching appears to be destabilizing. Figure 2*d* shows an example of the growth of a unit initial vector as the iteration progresses; while a mean growth rate can certainly be detected, there are significant fluctuations. We shall see this phenomenon again in the example of § 3.

(b) T as a passage time near a heteroclinic cycle

Our chief interest lies in understanding the effects of noise on (2.1) when A is a known function of the state of the underlying dynamical system (subject to transverse instability), which we represent by $\mathbf{x} \in \mathbb{R}^N$, so that $A = A(\mathbf{x}(t))$. We further suppose that in the absence of noise \mathbf{x} is attracted to a heteroclinic cycle joining points \mathbf{x}_1 and \mathbf{x}_2 , and that $A(\mathbf{x}_1) = A_1$, $A(\mathbf{x}_2) = A_2$ (cf. (2.2)). This supposes that the dynamics near \mathbf{x}_1 and \mathbf{x}_2 are essentially identical; it is easy to extend the theory below to the case when these are different.

We require a formula giving the passage time T near a equilibrium point (either \mathbf{x}_1 or \mathbf{x}_2) when the dynamical system is perturbed by a small amount of noise, taken here to have rms value ε . The appropriate result has been given by Stone & Holmes

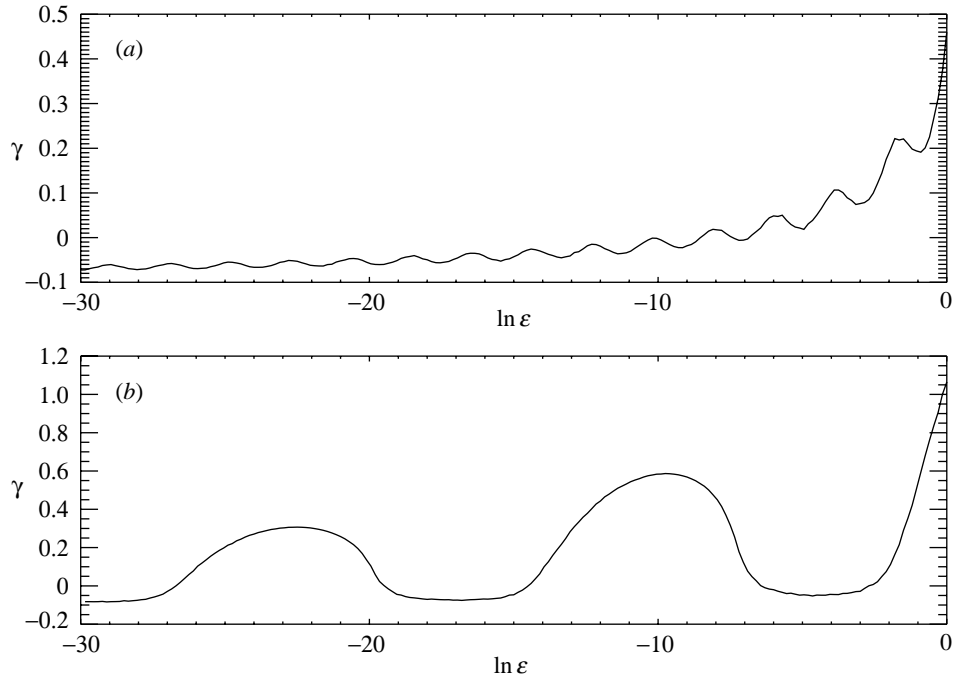


Figure 4. Growth rate plotted as a function of $\ln \varepsilon$ for the stochastically switched system with $a = 3.0$, $\lambda = 0.1$ and (a) $\delta = 2.0$, $\lambda_u = 2.0$; (b) $\delta = 500.0$, $\lambda_u = 12.0$. For each value of ε the growth rate is averaged over 5000 trials.

(1990; see also Lythe & Proctor 1993); they show that

$$P(T > S) = \text{erf}(\Delta(S)), \quad (2.16)$$

where

$$\Delta(S) = \delta \left(\frac{\varepsilon^2}{\lambda_u} (e^{2\lambda_u S} - 1) \right)^{-1/2}, \quad (2.17)$$

δ is an $\mathcal{O}(1)$ constant and λ_u is the real part of the most unstable eigenvalue within the invariant subspace near the equilibrium point. Thus we may regard T as a random variable with the probability density function

$$f(S) = -\frac{d}{dS}(\text{erf}(\Delta(S))) = \frac{2\lambda_u \Delta(S) e^{-\Delta^2(S)}}{\sqrt{\pi}(1 - e^{-2\lambda_u S})}. \quad (2.18)$$

We now investigate the dynamics of (2.1), (2.2) where the switching intervals $T_n - T_{n-1}$ are not fixed but are drawn from the distribution (2.18). In figure 3 we show examples of $f(S)$ for $\varepsilon = 10^{-2}$ and (a) $\delta = 2.0$, $\lambda_u = 2.0$; (b) $\delta = 500.0$, $\lambda_u = 12.0$. In the first case the switching time is peaked at 3, with a standard deviation of order unity, while in the second case the peak occurs at *ca.* 1.05 with standard deviation of order 0.2. The method by which the distribution is sampled is given in Appendix A.

We fix λ_u and δ and integrate the equations $\dot{\mathbf{z}} = A_1 \mathbf{z}$, $\dot{\mathbf{z}} = A_2 \mathbf{z}$ alternately for times T_1, T_2 , etc., until a mean growth/decay rate of the solution can be estimated

with sufficient accuracy. This mean growth rate can then be investigated as a function of the noise level. The results are displayed in figure 4*a* for $\lambda_u = \delta = 2.0$, and in figure 4*b* for $\lambda_u = 12.0$, $\delta = 500.0$. The first of these figures bears little resemblance to the zero-variance case of figure 2*a*. This is because there is a characteristic time-scale T_r of order unity associated with the rotatory part of the matrices A_1, A_2 ; this time must be compared with ΔT_f , the standard deviation of the distribution $f(S)$, which is essentially independent of ε , and the mean passage time \bar{T} , which for small ε is approximately $-(1/\lambda_u) \ln \varepsilon$. In figure 4*a*, $T_r \sim \Delta T_f$ and so it cannot be expected that a constant-time model would give accurate results. In contrast, for figure 4*b* $T_r \gg \Delta T_f$ and so, as one might expect, the distribution of growth rate with $\ln \varepsilon$ closely resembles figure 2*a* (reversed, since \bar{T} decreases as ε increases).

We can thus see that for this very simple model problem the effects of noise are well modelled by the regular switching model only when the variance is small. In both the small- and the large-variance cases, however, the numerical results show that so long as the noiseless system is not too stable, the noisy system can be destabilized by the disturbance. Thus the simple model gives us the confidence to investigate, using similar ideas, a convective dynamo that owes its existence to stochastic perturbation.

3. A stochastically excited dynamo

We now turn to the main part of the paper—the demonstration of dynamo action in non-rotating thermal convection in a layer. The basic model problem is that used for many years to model magnetoconvection in three dimensions (see, for example, Matthews *et al.* 1996), with the crucial difference that no mean magnetic flux is imposed on the system: thus any sustained magnetic field must be due to self-excitation, or *dynamo action* (for an introduction to the fundamentals of dynamo theory, see Proctor & Gilbert (1994)).

Our physical model is as follows. A layer of perfect gas is bounded above and below by horizontal boundaries, considered to be stress-free and perfect heat conductors. The magnetic field is constrained to be vertical at the top and bottom boundaries. A fixed and uniform temperature difference is imposed between the boundaries. All quantities are supposed periodic in the two horizontal directions (x, y): there is no mean horizontal momentum. In dimensionless form the governing equations are (see, for example, Proctor & Weiss 1982)

$$\sigma^{-1} \left(\frac{\partial \mathbf{u}}{\partial t} + \mathbf{u} \cdot \nabla \mathbf{u} \right) = -\nabla p + Ra\theta \hat{\mathbf{z}} + \nabla^2 \mathbf{u} + \zeta Q (\nabla \times \mathbf{B}) \times \mathbf{B}, \quad (3.1)$$

$$\frac{\partial \theta}{\partial t} + \mathbf{u} \cdot \nabla \theta = \nabla^2 \theta, \quad \nabla \cdot \mathbf{u} = 0, \quad (3.2)$$

$$\frac{\partial \mathbf{B}}{\partial t} - \nabla \times (\mathbf{u} \times \mathbf{B}) = \zeta \nabla^2 \mathbf{B}, \quad \nabla \cdot \mathbf{B} = 0, \quad (3.3)$$

where \mathbf{u} is the fluid velocity, θ is the temperature perturbation from the static conduction state ($\theta = 0$ at the top and bottom of the layer), and \mathbf{B} is the magnetic field strength. The dimensionless parameters are the Rayleigh number Ra (proportional to the imposed temperature contrast), the Prandtl number σ (ratio of kinematic viscosity to thermal diffusivity), the ratio (ζ) of magnetic to thermal diffusivity, and ℓ , the aspect ratio of the box (supposed to have square cross-section). The fluid is incompressible and the Boussinesq approximation is used. For the time being the

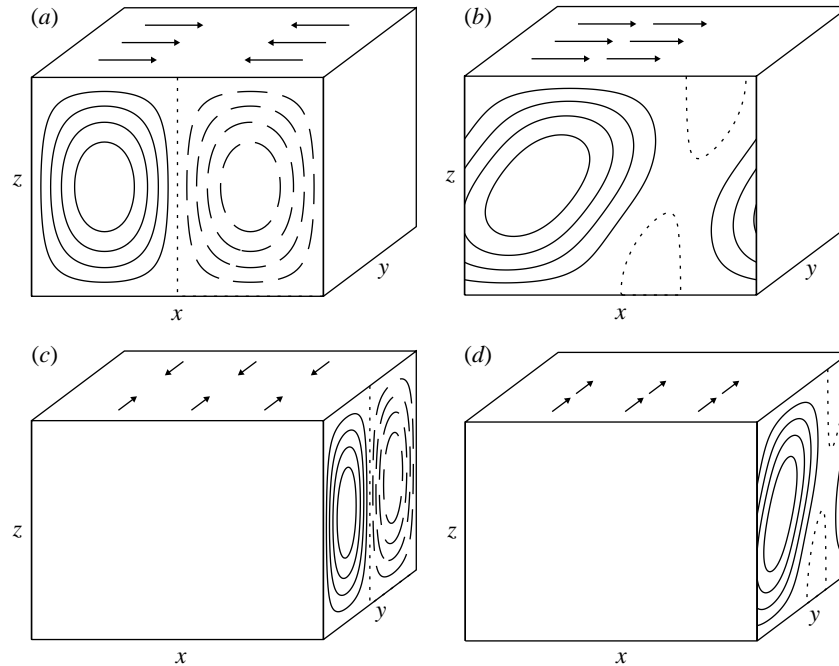


Figure 5. A structurally stable heteroclinic cycle connecting four equilibria: (a) x -rolls; (b) tilted x -rolls; (c) y -rolls; (d) tilted y -rolls, then returning to rolls. See also figure 6.

Chandrasekhar number Q , representing the magnitude of the magnetic energy, will be set to zero, so that there is no dynamical effect of the field on the flow. We note that in that case the system has a skew-product structure, with the (\mathbf{u}, θ) dynamics forcing the \mathbf{B} dynamics. Thus the induction equation (3.3), which is linear in \mathbf{B} , the magnetic field strength, plays the role of the transverse coordinate z in the simple model of §2, while the variation of the velocity \mathbf{u} with time provides the time-dependent coefficients of the linear stability problem.

There are many possible forms of convection that can occur for different values of the parameters. Of particular interest for our purposes is the time-dependent flow shown in figure 5, which has the desired form of a structurally stable heteroclinic cycle (see Matthews *et al.* 1996). The cycle connects four equilibrium points, which can be characterized as: (a) x -rolls, cellular motion in the (x, z) plane with no y -dependence; (b) tilted x -rolls, as (a) but now with a horizontal shear that enhances every other roll amplitude; (c) y -rolls; and (d) tilted y -rolls. Both (b) and (d) possess mirror images under reflection in a vertical plane, and the choice of which mirror image the cycle visits depends sensitively on the parameters. Each of the flows (a)–(d) has the property that the particle paths are all perpendicular to some fixed direction, and it has been shown that such flows cannot lead to the dynamo instability (see Roberts 1994). Nonetheless these flows can act on an initially weak magnetic field to increase its energy (proportional to $|\mathbf{B}|^2$) for a finite time before diffusion finally leads to exponential decay. This structurally stable cycle is of just the right form to be investigated by the methods of the previous section.

We do not work from the PDEs directly, but from a 44-equation set of ODEs derived from the PDEs by Fourier expansions and arbitrary truncation, which

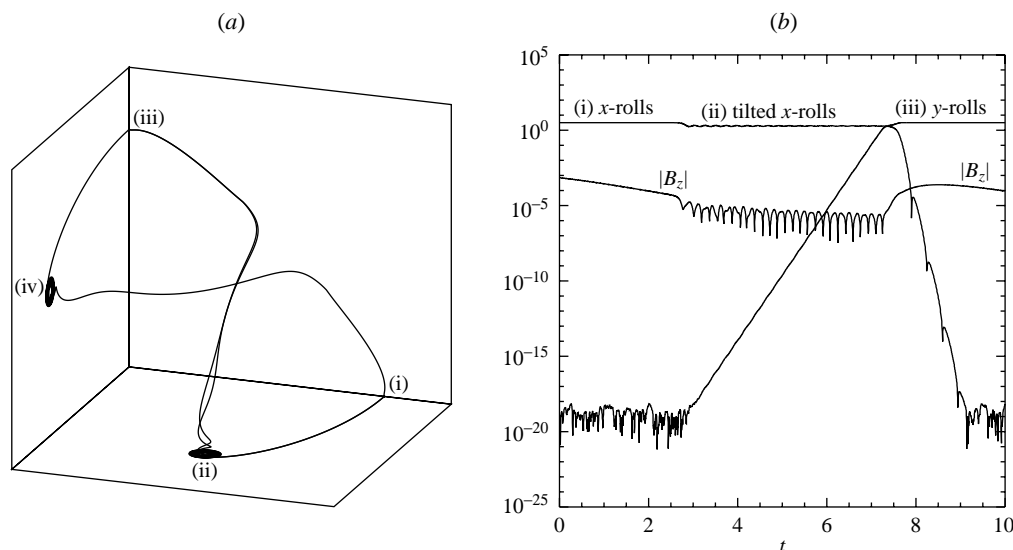


Figure 6. (a) Phase portrait of the structurally stable heteroclinic cycle shown in figure 5, with noise $\varepsilon = 10^{-20}$: (i)–(iv) in the figure denote the four equilibria: x -rolls, tilted x -rolls, y -rolls and tilted y -rolls. Points (i) and (iii) are saddles, while (ii) and (iv) are saddle foci. The three coordinate surfaces represent invariant subspaces of the problem. (b) Time-series, showing the amplitude of x -rolls and y -rolls against time. The trajectory starts at x -rolls, then switches to tilted x -rolls. At this point, the amplitude of y -rolls starts to grow exponentially; once it exceeds the amplitude of x -rolls, this drops rapidly to the noise level. The amplitude of $|B_z|$ (also shown) has transient growth as the trajectory reaches y -rolls.

have been shown to give a very good qualitative description of the non-magnetic dynamics—in particular, the PDE and ODE systems appear to possess structurally stable heteroclinic cycles for similar values of the parameters (Matthews *et al.* 1996). The system of ODEs used, and the method by which they are obtained, are described in Appendix B.

It is well known that the behaviour of numerical simulations of dynamos with steady velocity fields is very sensitive to the level of truncation (see, for example, Matthews 1999). While we have not carried out simulations that fully resolve magnetic boundary layers, which are important in the dynamo process, it is still the case that the convective states (equilibrium points) in the cycle have transverse dynamics given by non-normal matrices (see Appendix B), even when the magnetic field is fully resolved (cf. Hughes 1993), so we expect the mechanism we describe to lead to dynamo action.

Figure 6a shows a picture of the structurally stable cycle in a three-dimensional projection, while figure 6b shows a time-series of part of the cycle, plotting the amplitudes of x -rolls, y -rolls and $|B_z|$ (a measure of the distance from the invariant subspace $\mathbf{B} = 0$, and defined in Appendix B) against time. Note the transient growth of $|B_z|$ as the trajectory reaches y -rolls. We make a choice of parameters ($Ra = 6100.0$, $\sigma = 1.2$, $Q = 0.0$, $\zeta = 0.025$, $\ell = 1$) for which this cycle exists and is asymptotically stable in the absence of noise. We then integrate the governing equations, adding (at each time-step and to the right-hand side of each equation) normally distributed noise with zero mean and standard deviation ε . Figure 7 shows the growth of $|B_z|$

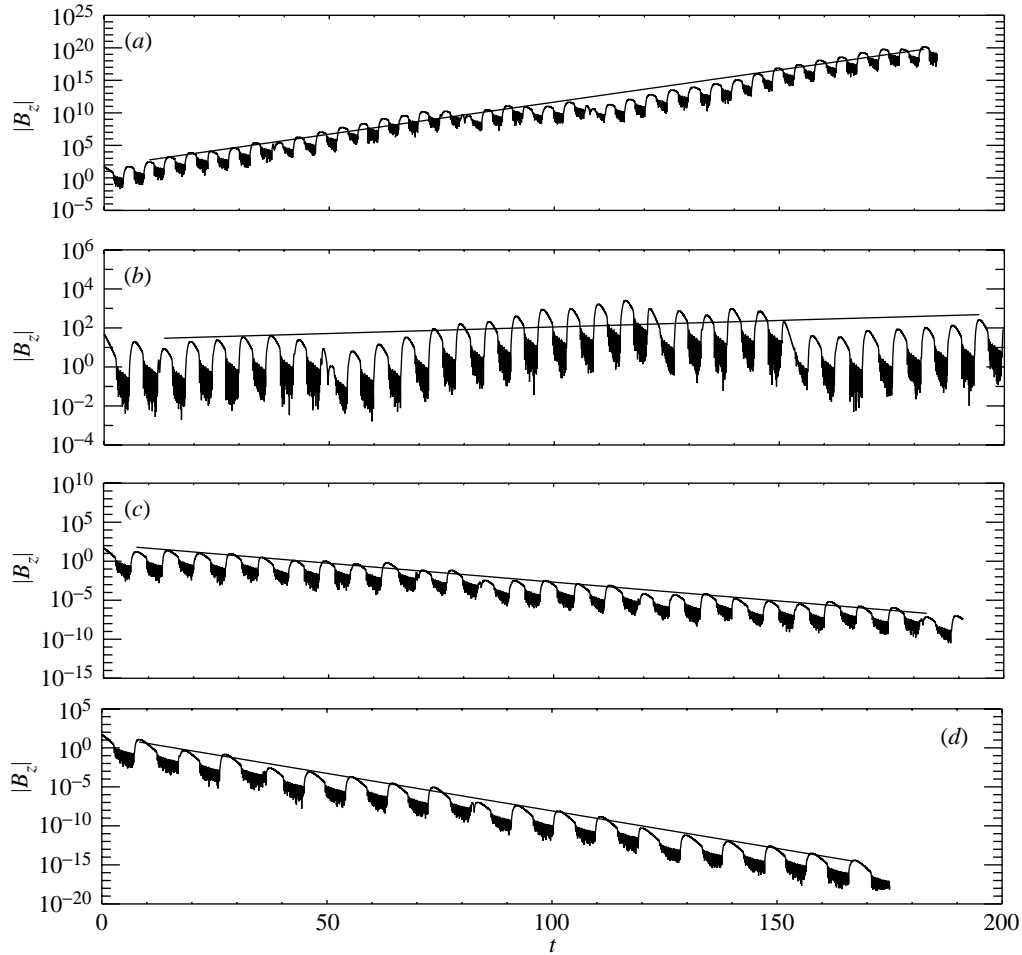


Figure 7. $|B_z|$ as a function of time. The straight lines are best fits to the average growth rates γ (shifted for clarity): (a) $\varepsilon = 10^{-10}$ ($\gamma = 0.23$); (b) $\varepsilon = 10^{-13}$ ($\gamma = 0.02$); (c) $\varepsilon = 10^{-15}$ ($\gamma = -0.11$); (d) $\varepsilon = 10^{-20}$ ($\gamma = -0.22$).

for various values of ε . It can be seen that the growth rate increases on average with increasing ε , although for larger values of ε there is considerable short-time variation. Figure 8 shows the ratio between successive peaks of $|B_z|$ for the oscillation against the time-interval between such peaks. There is considerable scatter, as one might expect, but there is a clear trend relating increasing time-interval to decreasing noise, leading to lower growth rates. Finally, in figure 9 we show a histogram of the distribution of time-intervals for the four different noise levels. As expected, the distributions all have the same approximate shape (though not height, since the sample sizes are different), which bears a good qualitative resemblance to the probability distribution of figure 3. There is no evidence of any oscillation in the growth rate as a function of noise, but this is perhaps not unexpected since the standard deviation is of the order of the cycle time, as discussed in the previous section. The effects of noise on this system are manifested only in the growth rate and the switch-

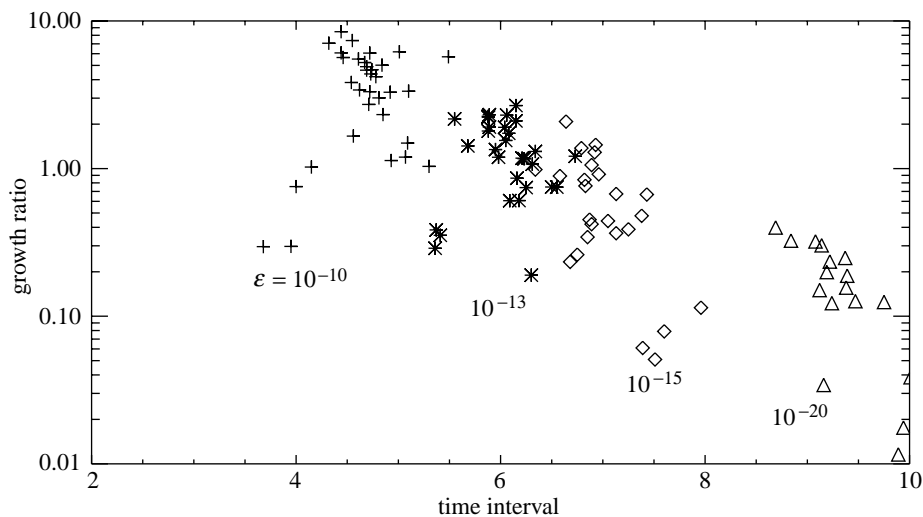


Figure 8. Ratio between successive major peaks in $|B_z|$ (see figure 7) of the oscillation against the time-interval between such peaks: +, $\varepsilon = 10^{-10}$; *, $\varepsilon = 10^{-13}$; \diamond , $\varepsilon = 10^{-15}$; \triangle , $\varepsilon = 10^{-20}$.

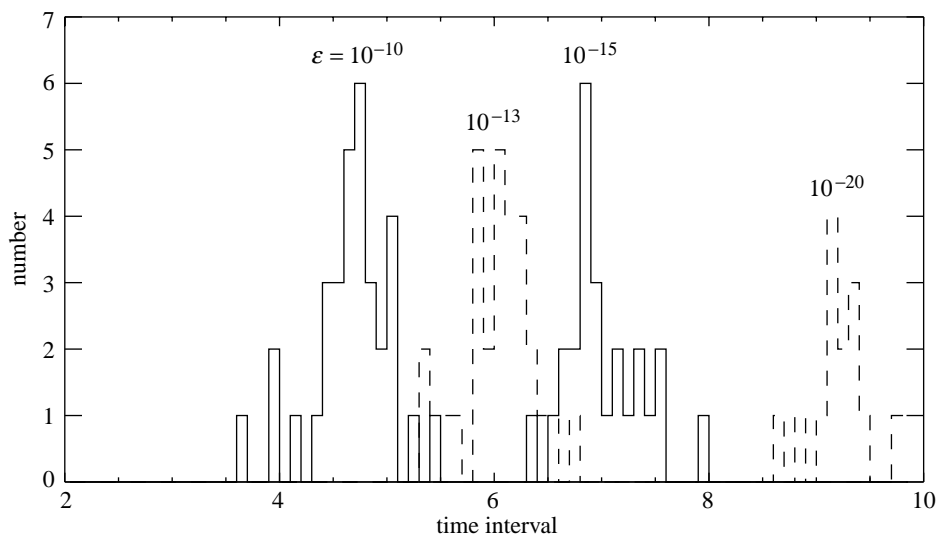


Figure 9. Histogram of the distribution of time intervals for the four different noise levels, as in figure 8.

ing intervals. At no time does the solution itself look ‘noisy’. The apparent irregular high-frequency oscillation in every cycle is a consequence of an oscillatory approach to the equilibrium points representing the tilted cells (see figure 6).

4. Discussion

We have shown how added noise can destabilize transverse modes when the trajectories in an invariant subspace lie close to a heteroclinic cycle. Transverse instability can occur even when each equilibrium point of the cycle is associated with decay-

ing eigenfunctions. Non-normality of the transverse dynamics favours the instability, since the instability mechanism depends on constructive interactions between transiently growing solutions. In some ways the mechanism is similar to parametric instability, although with a crucial stochastic component. The particular application described in § 3 is of some interest since it is an example of dynamo action in a convective problem with reflectional symmetry, at least on average. This distinguishes it importantly from other convective dynamos, which rely on rotation of the layer to be effective.

There are other mechanisms by which the addition of noise can destabilize non-normal systems. An interesting example is given by Farrell & Ioannou (1994), who show that a subcritical mode can be destabilized by the addition of relatively small amounts of noise to a non-normal system. Our mechanism is completely different, however, in that it is entirely linear: the addition of sufficient noise leads to indefinite exponential growth of the transverse modes.

Heteroclinic cycles arise in a variety of other convection problems, and there has been considerable interest in the dynamo instability of heteroclinic cycles that occurs in rotating plane-layer convection (Chossat *et al.* 1999a; Jones & Roberts 1999; Matthews 1999) and in spherical shell convection (Chossat *et al.* 1999b; Oprea *et al.* 1997). In these papers, the authors have been concerned with situations in which the states that make up the cycle are themselves unstable to dynamo action, in contrast to the situation discussed here, where the instability of the cycle is noise driven.

The main effect of the noise is to prevent the cycle time of trajectories approaching the heteroclinic cycle from going to infinity. There are other ways of achieving this which do not involve the addition of noise: for example, the effect of a small (but deterministic) perturbation that breaks some, but not all, of the symmetries of a problem may be to transmute a heteroclinic cycle into a different heteroclinic cycle or indeed to a long-period periodic orbit (cf. Chossat *et al.* 1999b; Sandstede & Scheel 1995).

We end with a final word of warning about the nonlinear development of the instability. While it is easy to invent, for the simple problem of § 2, types of nonlinearity that result in the equilibration of the solution at small amplitude, the situation is not always so straightforward. As an example consider our convective problem, but now with $Q = 1$, so that the magnetic (Lorentz) forces have an effect on the flow if the field is strong enough. In this case for finite magnetic field the solution bears no resemblance to the non-magnetic solution: figure 10 is the dynamic analogue of figure 6a! Once the cycle has been destabilized by noise and the field grows to finite amplitude, the noise may be set to zero without relaminarization occurring.

J.R.G. was supported by the UK EPSRC, I.O. was partly supported by the EU TEMPUS programme and A.M.R. was supported by the Royal Astronomical Society. We thank D. P. Brownjohn for computational assistance and R. S. Mackay and I. S. Melbourne for helpful discussions.

Appendix A. Construction of the conditional distribution function

To generate values of T with the probability distribution function $f(S)$ (2.18) we use the cumulative distribution function

$$P(T > S) = \text{erf}(\Delta(S)) \equiv \Theta(S) \quad (\text{A } 1)$$

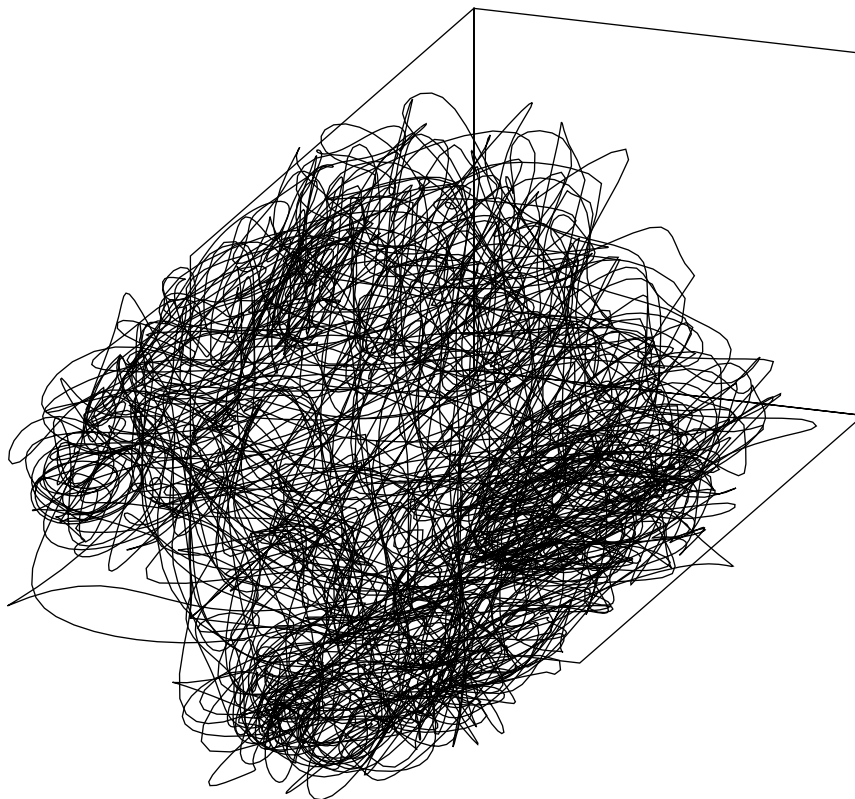


Figure 10. Chaotic trajectory for the same parameter values as in figure 6, but including the dynamical effect of the magnetic field ($Q = 1$).

defined in (2.16). One way of proceeding would be to generate random values for Θ uniformly over $[0, 1]$, and then invert to give a value of T for each Θ . This is lengthy, however, and instead we use the following method. We note first that the function $\Delta(S)$ can be inverted explicitly:

$$\Delta^{-1}(\xi) = \frac{1}{2\lambda_u} \ln \left(\lambda_u \left(\frac{\delta}{\varepsilon\xi} \right)^2 + 1 \right), \quad S(\Theta) = \Delta^{-1}(\text{erf}^{-1}(\Theta)). \quad (\text{A } 2)$$

We then pick a thousand evenly spaced values of $\Theta \in [0, 1)$ and find the inverse error function values (this need be done only once). These are then stored, and the form of the distribution function is then found by choosing at random one of these precalculated values and applying Δ^{-1} , which does depend on the parameters. The comparison of the resulting histogram with the calculated probability distribution function is satisfactory, as seen in figure 3.

Appendix B. Truncation of the dynamo PDEs

The procedure of truncation and determining the ODEs satisfied by the amplitudes of the 44 modes is straightforward but time-consuming, so we present the process in outline only; the full set of ODEs is available from the authors. This truncation was

originally carried out by Rucklidge & Matthews (1995) using the symbolic algebra package REDUCE (Hearne 1991).

We represent solutions of the PDEs (3.1)–(3.3) using a minimal Galerkin truncation of 44 Fourier modes (15 for velocity \mathbf{u} , eight for temperature θ and 21 for the magnetic field \mathbf{B}):

$$u_z/k = (u_{101} \cos kx + u_{011} \cos ky) \sin \pi z + (u_{102} \sin kx + u_{012} \sin ky) \sin 2\pi z + u_{112} \cos kx \cos ky \sin 2\pi z + 4 \text{ more}, \quad (\text{B } 1)$$

$$u_x/\pi = -u_{101} \sin kx \cos \pi z + 2u_{102} \cos kx \cos 2\pi z + u_{x01} \cos \pi z - u_{112} \sin kx \cos ky \cos 2\pi z + 4 \text{ more}, \quad (\text{B } 2)$$

$$u_y/\pi = -u_{011} \sin ky \cos \pi z + 2u_{012} \cos ky \cos 2\pi z + u_{0y1} \cos \pi z - u_{112} \cos kx \sin ky \cos 2\pi z + 4 \text{ more}, \quad (\text{B } 3)$$

$$\theta = (\theta_{101} \cos kx + \theta_{011} \cos ky) \sin \pi z + (\theta_{102} \sin kx + \theta_{012} \sin ky) \sin 2\pi z + (\theta_{002} + \theta_{112} \cos kx \cos ky) \sin 2\pi z + 2 \text{ more}, \quad (\text{B } 4)$$

$$B_z/k = (B_{101} \cos kx + B_{011} \cos ky) \cos \pi z + \pi(B_{z100} \sin kx + B_{z010} \sin ky)/k + 2(B_{102} \sin kx + B_{012} \sin ky) \cos 2\pi z + 9 \text{ more}, \quad (\text{B } 5)$$

$$B_x/\pi = B_{101} \sin kx \sin \pi z - 4B_{102} \cos kx \sin 2\pi z - B_{x01} \sin \pi z + 5 \text{ more}, \quad (\text{B } 6)$$

$$B_y/\pi = B_{011} \sin ky \sin \pi z - 4B_{012} \cos ky \sin 2\pi z - B_{0y1} \sin \pi z + 5 \text{ more}, \quad (\text{B } 7)$$

where $k = 2\pi/\ell$ and the amplitudes u_{101} , etc., are functions of time. The modes u_{101} , θ_{101} and B_{101} represent two-dimensional convection rolls with their axes aligned in the y -direction; u_{102} , θ_{102} and B_{102} represent modes that cause the rolls to tilt; and u_{x01} and B_{x01} represent a shear across the layer. Similarly at 90° , we have u_{011} , etc. The mode θ_{002} represents the perturbation to the horizontally averaged temperature; u_{112} and θ_{112} represent nonlinear interactions between the two sets of rolls; and B_{z100} and B_{z010} represent how the vertical magnetic field is expelled from the convecting regions. The modes not written explicitly are generated by nonlinear interactions between the modes described here, and typically involve vertical vorticity and vertical current.

Rather than work with the PDEs (3.1)–(3.3), we use the temperature equation (3.2), the z components of the momentum (3.1) and induction (3.3) equations, and the z components of the curls of these last two equations. The expansions above are inserted into these five PDEs and the system is truncated to give a set of ODEs for the amplitudes of each mode. In abbreviated form, these are

$$\dot{u}_{101} = -\sigma k_{11}^2 u_{101} + \frac{k}{k_{11}^2} \sigma Ra \theta_{101} + \frac{1}{4} k \pi u_{011} u_{112} - \frac{k \pi k_{13}^2}{2k_{11}^2} u_{102} u_{x01} + \frac{\pi}{k_{11}^2} \sigma \zeta Q (+k k_{13}^2 B_{102} B_{x01} + \pi k_{-11}^2 B_{z100} B_{x01}), \quad (\text{B } 8)$$

$$\dot{u}_{102} = -\sigma k_{14}^2 u_{102} + \frac{k}{k_{14}^2} \sigma Ra \theta_{102} + \frac{k^3 \pi}{2k_{14}^2} (u_{101} u_{x01} + \sigma \zeta Q B_{101} B_{x01}), \quad (\text{B } 9)$$

$$\dot{u}_{x01} = -\sigma \pi^2 u_{x01} + \frac{3}{4} k \pi u_{101} u_{102} + \sigma \zeta Q (\frac{1}{2} \pi^2 B_{101} B_{z100} - \frac{3}{2} k \pi B_{101} B_{102}), \quad (\text{B } 10)$$

$$\dot{u}_{112} = -2\sigma k_{12}^2 u_{112} + \frac{k}{k_{12}^2} \sigma Ra \theta_{112} - \frac{k k_{11}^2 \pi}{k_{12}^2} (u_{101} u_{011} + \sigma \zeta Q B_{101} B_{011}), \quad (\text{B } 11)$$

$$\dot{\theta}_{101} = k u_{101} - k_{11}^2 \theta_{101} + k \pi u_{101} \theta_{002} + \frac{1}{4} k \pi u_{011} \theta_{112} - \frac{1}{2} k \pi u_{x01} \theta_{102}, \quad (\text{B } 12)$$

$$\dot{\theta}_{002} = -4\pi^2\theta_{002} - \frac{1}{2}k\pi(u_{101}\theta_{101} + u_{011}\theta_{011}), \quad (\text{B } 13)$$

$$\dot{\theta}_{102} = \frac{1}{2}k\pi u_{102} - k_{14}^2\theta_{102} + \frac{1}{2}k\pi u_{x01}\theta_{101}, \quad (\text{B } 14)$$

$$\dot{\theta}_{112} = ku_{112} - 2k_{12}^2\theta_{112} - \frac{1}{2}k\pi(u_{101}\theta_{011} + u_{011}\theta_{101}), \quad (\text{B } 15)$$

$$\dot{B}_{101} = -k_{11}^2\zeta B_{101} + \frac{1}{4}k\pi u_{112}B_{011} - \frac{1}{2}k\pi(2u_{x01}B_{102} + u_{102}B_{x01}) - \pi^2 u_{x01}B_{z100}, \quad (\text{B } 16)$$

$$\dot{B}_{x01} = -\pi^2\zeta B_{x01} + \frac{1}{4}k\pi(u_{102}B_{101} + 2u_{101}B_{102}) - \frac{1}{2}\pi^2 u_{101}B_{z100}, \quad (\text{B } 17)$$

$$\dot{B}_{102} = -k_{14}^2\zeta B_{102} + \frac{1}{4}k\pi(u_{x01}B_{101} - u_{101}B_{x01}), \quad (\text{B } 18)$$

$$\dot{B}_{z100} = -k^2\zeta B_{z100} + \frac{1}{2}k^2(u_{x01}B_{101} + u_{101}B_{x01}), \quad (\text{B } 19)$$

where $k_{mn}^2 = mk^2 + n\pi^2$, and equations for u_{011} , etc., can be deduced from the above. Note that these are not the full set of 44 equations that were used in §3, but are presented in abbreviated form in order to illustrate the structure of the full set of ODEs. These equations include as subsystems or as special cases the Lorenz (1963) equations as well as truncations presented by Kennett (1976) and Howard & Krishnamurti (1986). If a mean vertical magnetic field is introduced (this has the effect of including linear interactions between the velocity and magnetic field modes), we recover truncations presented by Knobloch *et al.* (1981) and by Rucklidge & Matthews (1996).

The equilibrium point representing x -rolls has u_{101} , θ_{101} and θ_{002} non-zero, while tilted x -rolls have u_{102} , u_{x01} , θ_{102} non-zero as well. The dynamics of the magnetic field near x -rolls is then described by the linear system

$$\begin{pmatrix} \dot{B}_{x01} \\ \dot{B}_{102} \\ \dot{B}_{z100} \end{pmatrix} = \begin{bmatrix} -\pi^2\zeta & \frac{1}{2}k\pi u_{101} & -\frac{1}{2}\pi^2 u_{101} \\ -\frac{1}{4}k\pi u_{101} & -k_{14}^2\zeta & 0 \\ \frac{1}{2}k^2 u_{101} & 0 & -k^2\zeta \end{bmatrix} \begin{pmatrix} B_{x01} \\ B_{102} \\ B_{z100} \end{pmatrix}, \quad (\text{B } 20)$$

with a related expression for the dynamics near the tilted x -roll equilibrium point. The above matrix is non-normal (with $u_{101} \approx 3.3$ at the equilibrium point, $\zeta = 0.025$ and $k = 2\pi$), and it has one real and two complex eigenvalues. The real eigenvalue and real parts of the complex eigenvalues are all negative and go to zero roughly as ζ , while the imaginary parts of the complex eigenvalues are roughly independent of ζ , consistent with the discussion in §2.

Finally, we define $|B_z|$ by

$$|B_z|^2 = B_{z100}^2 + B_{z010}^2 + 4 \text{ more}, \quad (\text{B } 21)$$

since these modes prove to be the most slowly decaying after each transition from tilted rolls to rolls, and so $|B_z|$ gives a measure of the distance from the $\mathbf{B} = 0$ subspace that does not oscillate too wildly.

References

- Ashwin, P., Buescu, J. & Stewart, I. 1996 From attractor to chaotic saddle: a tale of transverse instability *Nonlinearity* **9**, 703–737.
- Chossat, P., Krupa, M., Melbourne, I. & Scheel, A. 1997 Transverse bifurcations of homoclinic cycles. *Physica D* **100**, 85–100.
- Chossat, P., Krupa, M., Melbourne, I. & Scheel, A. 1999a Magnetic dynamos in rotating convection: a dynamical systems approach. *Dyn. Cont. Discr. Impulsive Syst.* **5**, 327–340.

- Chossat, P., Guyard, F. & Lauterbach, R. 1999*b* Generalized heteroclinic cycles in spherically invariant systems and their perturbations. *J. Nonlin. Sci.* **5**, 479–524.
- Farrell, B. F. & Ioannou, P. J. 1994 Variance maintained by stochastic forcing of non-normal dynamical systems associated with linearly stable shear flows. *Phys. Rev. Lett.* **72**, 1188–1191.
- Hearne, A. C. 1991 *REDUCE user's manual*, ver. 3.4. Santa Monica, CA: Rand.
- Howard, L. N. & Krishnamurti, R. 1986 Large-scale flow in turbulent convection: a mathematical model. *J. Fluid Mech* **170**, 385–410.
- Hughes, D. W. 1993 Testing for dynamo action. In *Solar and planetary dynamos* (ed. M. R. E. Proctor, P. C. Matthews & A. M. Rucklidge), pp. 153–159. Cambridge University Press.
- Jones, C. A. & Roberts, P. H. 1999 Convection driven dynamos in a rotating plane layer. *J. Fluid Mech.* (In the press.)
- Kennett, R. G. 1976 A model for magnetohydrodynamic convection relevant to the solar dynamo problem. *Stud. Appl. Math.* **55**, 65–81.
- Knobloch, E., Weiss, N. O. & Da Costa, L. N. 1981 Oscillatory and steady convection in a magnetic field. *J. Fluid Mech.* **113**, 153–186.
- Krupa, M. & Melbourne, I. 1995 Asymptotic stability of heteroclinic cycles in systems with symmetry. *Ergod. Theory Dynam. Syst.* **15**, 121–147.
- Lorenz, E. N. 1963 Deterministic nonperiodic flow. *J. Atmos. Sci.* **20**, 130–141.
- Lythe, G. D. & Proctor, M. R. E. 1993 Noise and slow-fast dynamics in a three-wave resonance problem. *Phys. Rev. E* **47**, 3122–3127.
- Matthews, P. C. 1999 Dynamo action in simple convective flows. *Proc. R. Soc. Lond. A* **455**, 1829–1840.
- Matthews, P. C., Rucklidge, A. M., Weiss, N. O. & Proctor, M. R. E. 1996 The three-dimensional development of the shearing instability of convection. *Phys. Fluids* **8**, 1350–1352.
- Oprea, I., Chossat, P. & Armbruster, D. 1997 Simulating the kinematic dynamo forced by heteroclinic convective velocity fields. *Theor. Comput. Fluid Dynam.* **9**, 293–309.
- Proctor, M. R. E. & Gilbert, A. D. 1994 *Lectures on solar and planetary dynamos*. Cambridge University Press.
- Proctor, M. R. E. & Weiss, N. O. 1982 Magnetoconvection. *Rep. Prog. Phys.* **45**, 1317–1379.
- Roberts, P. H. 1994 Fundamentals of dynamo theory. In *Lectures on solar and planetary dynamos* (ed. M. R. E. Proctor & A. D. Gilbert), pp. 257–264. Cambridge University Press.
- Rucklidge, A. M. & Matthews, P. C. 1995 The shearing instability in magnetoconvection. In *Double-diffusive convection* (ed. A. Brandt & H. J. S. Fernando), pp. 171–184. Washington, DC: American Geophysical Union.
- Rucklidge, A. M. & Matthews, P. C. 1996 Analysis of the shearing instability in nonlinear convection and magnetoconvection. *Nonlinearity* **9**, 311–351.
- Sandstede, B. & Scheel, A. 1995 Forced symmetry breaking of homoclinic cycles. *Nonlinearity* **8**, 333–365.
- Stone, E. & Holmes, P. 1990 Random perturbations of heteroclinic attractors. *SIAM Jl Appl. Math.* **50**, 726–743.
- Trefethen, L. N. 1997 Pseudospectra of linear operators. *SIAM Rev.* **39**, 383–406.